NANO LETTERS

Letter

pubs.acs.org/NanoLett

Shape Engineering Driven by Selective Growth of SnO_2 on Doped Ga_2O_3 Nanowires

Manuel Alonso-Orts,[†] Ana M. Sánchez,*[,‡] Steven A. Hindmarsh,[‡] Iñaki López,[†] Emilio Nogales,[†] Javier Piqueras,[†] and Bianchi Méndez*[,†,‡]

[†]Departamento de Física de Materiales, Facultad de Ciencias Físicas, Universidad Complutense de Madrid, 28040-Madrid, Spain

[‡]Department of Physics, University of Warwick, Coventry, CV4 7AL, United Kingdom

S *Supporting Information*

ABSTRACT: Tailoring the shape of complex nanostructures requires control of the growth process. In this work, we report on the selective growth of nanostructured tin oxide on gallium oxide nanowires leading to the formation of SnO_2/Ga_2O_3 complex nanostructures. Ga_2O_3 nanowires decorated with either crossing SnO_2 nanowires or SnO_2 particles have been obtained in a single step treatment by thermal evaporation. The reason for this dual behavior is related to the growth direction of trunk Ga_2O_3 nanowires. Ga_2O_3 nanowires grown along the [001] direction favor the formation of crossing SnO_2 nanowires. Alternatively, SnO_2 forms rhombohedral particles on [110] Ga_2O_3 nanowires leading to skewer-like structures. These complex oxide structures were grown by a catalyst-free vapor−solid process. When pure Ga and tin oxide were used as source materials and compacted powders of Ga_2O_3 acted as substrates, [110] Ga_2O_3 nanowires grow preferentially. High-resolution transmission electron microscopy analysis reveals epitaxial relationship lattice matching between the Ga_2O_3 axis and SnO_2 particles, forming skewer-like structures. The addition of chromium oxide to the source materials modifies the growth direction of the trunk Ga_2O_3 nanowires, growing along the [001], with crossing SnO_2 wires. The SnO_2/Ga_2O_3 junctions does not meet the lattice matching condition, forming a grain boundary. The electronic and optical properties have been studied by XPS and CL with high spatial resolution, enabling us to get both local chemical and electronic information on the surface in both type of structures. The results will allow tuning optical and electronic properties of oxide complex nanostructures locally as a function of the orientation. In particular, we report a dependence of the visible CL emission of SnO_2 on its particular shape. Orange emission dominates in SnO_2/Ga_2O_3 crossing wires while green-blue emission is observed in SnO_2 particles attached to Ga_2O_3 trunks. The results show that the Ga_2O_3−SnO_2 system appears to be a benchmark for shape engineering to get architectures involving nanowires via the control of the growth direction of the nanowires.

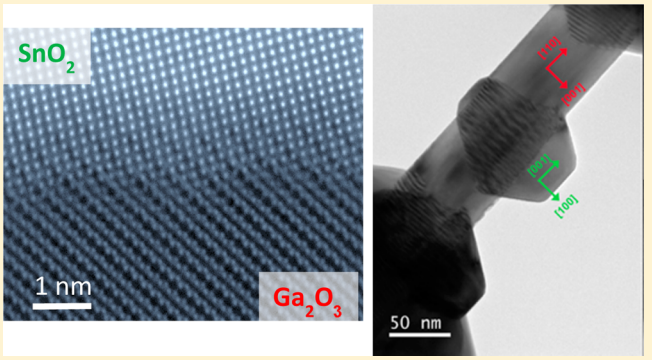

KEYWORDS: *Complex oxide nanowires, selective growth, crossed nanowires, transmission electron microsopy, cathodoluminescence*

Advances in smart nanostructured materials require a deep understanding of the growth mechanisms to develop novel designs and architectures. Engineering new architectures will enable the combination of zero-, one- and two-dimensional systems enhancing the functionalities in comparison with their single counterparts (quantum dots, nanowires, or nanosheets).[1] Some physical properties, such as optical and transport properties, could be strongly dependent on the morphology of nanomaterials, hence nanomaterials with mixed dimensionality could offer extra applications. For example, light emission in nanowires may be affected if nanowires are assembled with quantum dots in the same nanostructure.[2] Beside dimensionality, we can even broaden out the tailoring capabilities of nanostructured materials by mixing several chemical elements or compounds. For instance, 1D-TiO_2/2D-$ZnIn_2S_4$ nanostructures with improved photocatalytic properties have been very recently reported.[3] Semiconducting oxides are an attractive family of smart materials with wide range of morphologies within the quasi-one dimension (nanowires, nanobelts, or nanorods).[4] Besides, these oxides offer a high versatility in the following applications: optical and mechanical resonators, lasing, sensors, photocatalysis, solar cells, and biomedical and healthcare usages to name a few.[5−8] A great deal of research has been focused on synthesis, characterization, and applications of semiconducting oxide nanowires in the past decade, although there are still open questions. From the point of view of the physical properties, for example, it is still a challenge to get effectively doped oxide nanowires with controllable conductivity.[9] On the other hand, surface properties play a key role in the

Received: November 2, 2016
Revised: November 30, 2016
Published: December 21, 2016

ACS Publications © XXXX American Chemical Society

DOI: 10.1021/acs.nanolett.6b04189
Nano Lett. XXXX, XXX, XXX−XXX

case of nanomaterials due to the high aspect ratio of nanowires and nanoparticles. The surface influences both the physical−chemical properties and the growth mechanisms to generate specific architectures. Here, there is still room for improvement. In the case of Si nanowires, a model based on Plateau-Rayleigh instability has been recently proposed to generate one-dimensional Si−Ge heterostructures with modulation in their diameter. Surface energy considerations drive the growth while variations of kinetical parameters enable shape-tailoring.[10,11] Alternatively, in III−V nanowires surface energy engineering has been also exploited to control the polarity and the kink formation in III−V nanowires.[12] Hence, gaining knowledge about the relationship between crystal orientation and final morphology will contribute to understand the formation of nano-oxide assemblies and to get further control over their final shape.

Even though many works on hierarchical or complex nanostructures have been reported, most of semiconducting oxide nanomaterials refer to objects with homogeneous chemical composition, obtained from several routes.[13−15] In previous works, we have successfully grown a large variety of low-dimensional semiconducting oxide structures by thermal evaporation of chemical precursors under suitable thermal treatment parameters (gas flow and temperature). In particular, nanowires, nanotubes, or nanorods of ZnO, SnO_2, GeO_2, Sb_2O_3, In_2O_3, and Ga_2O_3, among others, with well-defined facets and high crystalline quality have already been reported.[16−19] In this work, we tackle the synthesis and characterization of some specific Ga_2O_3/SnO_2 architectures grown by a catalyst free vapor−solid (VS) mechanism. Monoclinic β-Ga_2O_3 and rutile SnO_2 are the thermodynamically stable phases of Ga_2O_3 and SnO_2, respectively. Their wide band gaps (4.9 and 3.7 eV, respectively) make them suitable for applications in the ultraviolet range. Their chemical stability, easiness of production and tune ability of physical properties make these oxides a potentially interesting alternative to other wide band gap semiconductors, such as the nitride family. Photodetectors and photocatalytic applications, as well as chemical sensors, batteries, light emitters, and energy applications have been anticipated using Ga_2O_3 or SnO_2 films and/or nanostructures.[20−23] In most of these applications, the surface plays a key role in the performance of the devices based on these oxides. The development of nanostructures combining these two oxides could be very promising from the point of view of applications. Ga_2O_3/SnO_2 heterostructures, which consisted of Sn-doped Ga_2O_3 and polycrystalline Ga-doped SnO_2 assembled in nanowires have been reported for sensing applications.[24] Also, Hsu and Lu reported the fabrication of Ga_2O_3/SnO_2 core−shell nanostructures with applications in ultraviolet detectors.[25] By using the above-mentioned VS catalyst free method, we have grown crossed Ga_2O_3/SnO_2 multiwire architecture and a detailed characterization of the heterojunctions has been carried out.[26] Here, we report the growth and characterization of two kinds of nanoheterostructures that have a main Ga_2O_3 nanowire axis: skewer-like (SK) structures with small SnO_2 particles attached to the trunk, and crossed wires (CW) structures consisting of SnO_2 wires cutting across a central Ga_2O_3 nanowire. The goal is to understand the underlying formation mechanisms and the main features of these heterostructures that could be extended to other oxide materials.

Single-step thermal treatments of metallic gallium along with tin oxide powders at 1500 °C for 15 h were conducted under argon flow in order to get conditions for the growth of both Ga_2O_3 and SnO_2 nanostructures. Alternatively, a small fraction of chromium oxide was added to the precursors and the same thermal treatment was carried out. Sn or Cr impurities have proved to increase the production yield of GeO_2 and Sb_2O_3 nanowires or nanorods during the thermal treatment, respectively.[27,28] It was previously found that with addition of a small amount of tin oxide powders to the Ga source, branched Ga_2O_3 nanowires were developed during a 1350 °C thermal treatment. Sn impurities were segregated toward the surface of the main Ga_2O_3 trunks during the thermal growth and became nucleation sites for secondary Ga_2O_3 branches.[29] In that case, the temperature was not enough to nucleate SnO_2 nanostructures. In the present work, the temperature has been increased up to 1500 °C. This temperature is closer to the melting point of SnO_2 and Ga_2O_3 (1630 and 1725 °C, respectively), which makes feasible the stabilization of both SnO_2 and Ga_2O_3 crystals.

In this work, two different heterostructures, skewer-like (Figure 1a) and crossed nanowires (Figure 1b), were analyzed in detail. Both are formed by a main longitudinal Ga_2O_3 nanowire with SnO_2 nanoparticles or transversal SnO_2

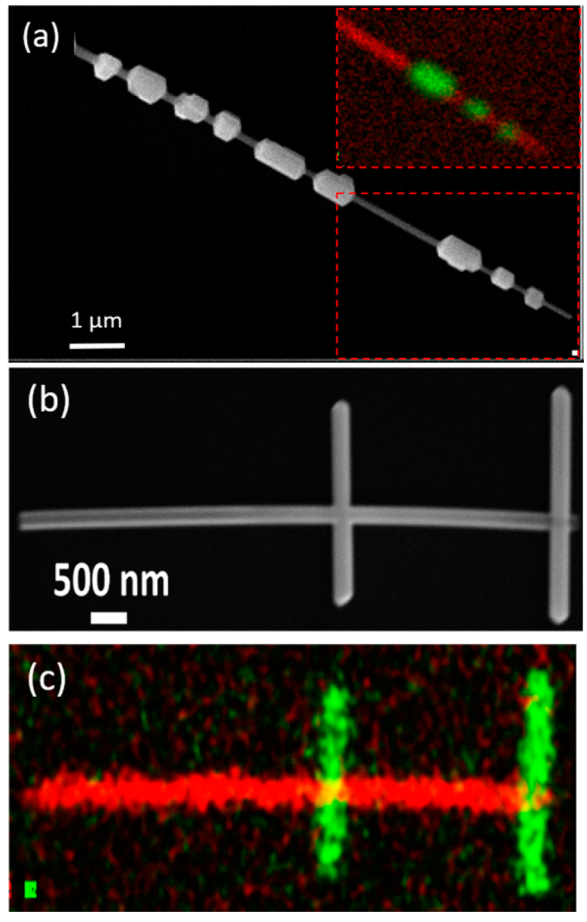

Figure 1. (a) SEM image of a skewer-like structure. Inset: the corresponding EDX map for Ga and Sn elements of the red square. Source materials were Ga chips and SnO_2 powders and the thermal treatment was carried out at 1500 °C for 15 h. (b) SEM image of several SnO_2 wires crossing a main Ga_2O_3 nanowire obtained after the addition of a small fraction of chromium oxide to the precursors and following the same thermal treatment as in (a) and (c) its corresponding EDX mapping of Sn (green) and Ga (red) elements.

DOI: 10.1021/acs.nanolett.6b04189
Nano Lett. XXXX, XXX, XXX−XXX

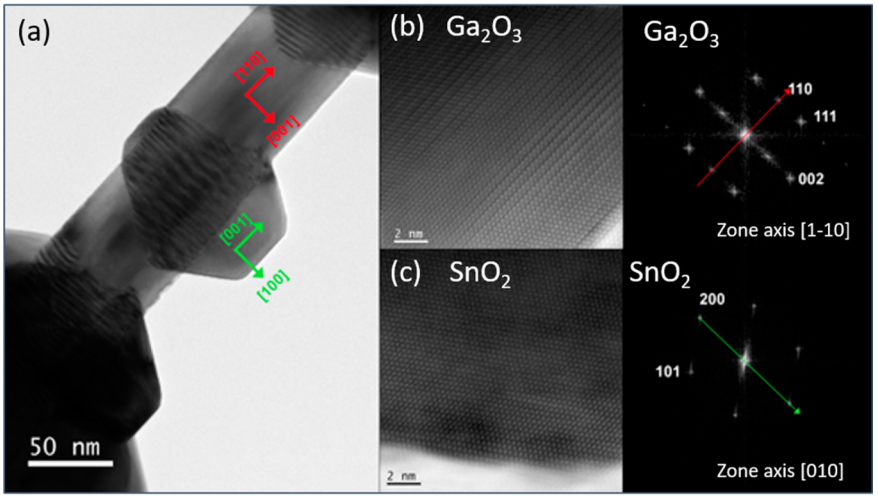

Figure 2. (a) TEM image of skewer-like structure. (b) HRTEM analysis of the Ga_2O_3 main axis of a skewer-like structure and its corresponding FT pattern. (c) HRTEM image of the SnO_2 particle and its FT pattern.

nanowire. The structure and morphology of these nanostructures were analyzed by high-resolution (scanning) transmission electron microscopy ((S)TEM) using JEOL 2100 and double-corrected ARM 200F microscopes working at 200 kV. Energy dispersive X-ray spectroscopy (EDX) analyses were performed with probe currents of approximately 200 pA and collected with an Oxford Instruments X-Max Silicon Drift Detector with an area of 100 mm^2. The microstructural characterization was correlated to physical and chemical properties by X-ray photoelectron spectroscopy (XPS) at Elettra synchrotron and by cathodoluminescence (CL) in the scanning electron microscope (SEM). A Leica Steroscan SEM and a JEOL 6100 were used for CL measurements. This information is very valuable to unravel the optical properties in oxides. In particular, our results shed some light into the luminescence bands of tin oxide affected by size-effects.

Figure 1a shows a general view of a representative SK structure in the SEM. This architecture consists of a Ga-containing trunk with thicknesses between 50−150 nm for different skewers, surrounded by Sn-containing rhombohedral-shaped particles as revealed by EDX (inset Figure 1a). The source materials, pure Ga and tin oxide powders, were placed on the top of a gallium oxide pellet, which acted as well as the substrate, into an open tubular furnace. Skewer-like structures were extensively produced after 15 h of thermal treatment under an argon gas flux of 0.8 l/min. A video composed by images taken at different times during growth is shown in the Supporting Information Video S1.

To determine the crystallographic relationship between trunk and nanoparticles, TEM analysis was carried out in the as-grown structures. Figure 2a shows a low-magnification bright-field TEM image of a skewer-like structure. Notice the presence of moiré fringes in the superposition of Sn-containing particles and the Ga-containing trunk. The moiré fringes indicate an epitaxial relationship between both components but with different lattice parameter and/or orientation. In particular, the observed translational moiré fringes (d_{tm}) in the SK structures arise from the slight misfit between Ga_2O_3 (110) planes (d_1) and SnO_2 (001) planes (d_2). This misfit could lead to some strain in the SnO_2 particles developed over the Ga_2O_3 wire. Figure S2 (Supporting Information) provides a TEM image of the trunk-particle junction between SnO_2 and Ga_2O_3 and its corresponding FFT pattern. The analysis of the translational moiré pattern observed gives a value of 4.07 nm. On the other hand, the theoretical expected value for the above-mentioned planes is 4.1 nm, which is quite close to the measured periodicity. This result suggests that the SnO_2 is relaxed at the very early stage of the growth. High-resolution TEM images were recorded in the trunk and the particles (Figure 2b,c, respectively) and the Fourier transform (FT) was enabled to identify the β-Ga_2O_3 phase and rutile SnO_2 for the trunk and nanoparticles, respectively. The Ga_2O_3 trunks grow along [110] and surface planes of the Ga_2O_3 NW are the (002) and the (1−10) planes. On the other hand, the SnO_2 particle attached to the NW exhibit facets of {101} type truncated by (200) planes. In Figure S3 (Supporting Information), a ball and stick model is shown that illustrates the lattice matching between (200) planes in SnO_2 and (002) planes of Ga_2O_3. The b lattice parameter of Ga_2O_3 is 3.04 Å while the c parameter of SnO_2 is 3.18 Å.

From these observations, the following formation mechanism of the SK structures is suggested. In the framework of a vapor−solid (VS) mechanism, the first condensed oxide molecules serve as nucleation sites in a self-catalytic scheme,where further deposition takes place leading to the formation of nanowires if there is a preferred growth direction.[30] In such a case, the minimization of free energy determines the directional growth during the condensation process, which is dominated by the surface energy growth of nanowires. This can be of crucial importance when it comes to anisotropic materials, as it is the case of the monoclinic β-Ga_2O_3 along the b direction.[31] Previous works have reported Ga_2O_3 NWs with several growth directions [010], [001], [110], or [40−1] obtained by different methods, such as chemical vapor deposition or thermal deposition, and usually in all these works a foreign metal catalyst has been used.[32,33] In the present work, Ga_2O_3 NWs are first formed by oxidation of the metallic Ga precursor under dynamical thermal conditions in the furnace. The growth conditions promotes the [110] growth direction for the Ga_2O_3 NWs. This orientation seems to be preferred in thin nanowires. The occurrence of a particular growth direction will give rise to a characteristic faceting of the final nanostructure, which is a key factor when it comes to the formation of more complex nanostructures. Here, the surface facets of the thin NWs favors

DOI: 10.1021/acs.nanolett.6b04189
Nano Lett. XXXX, XXX, XXX−XXX

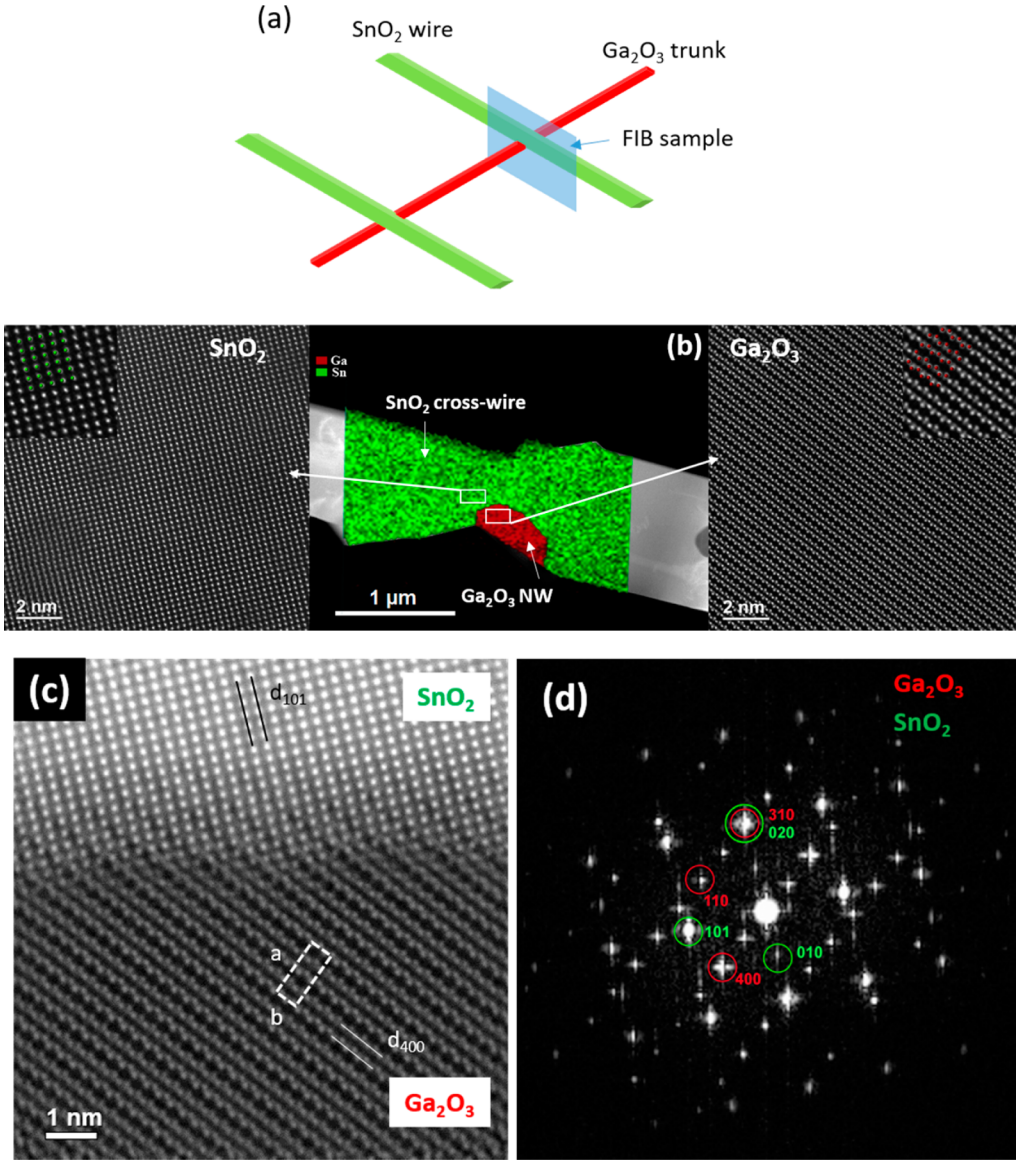

Figure 3. (a) Artwork depicting the cross-section of the junction area between SnO_2 and Ga_2O_3 nanowires prepared by focused ion beam technique. (b) TEM analysis of the cross-section area of crossing wires prepared by FIB (central image) overlapped with the compositional information provided by EDX (Ga in red, Sn in green). Left: high-resolution STEM of SnO_2 wire. Right: high-resolution STEM of the central Ga_2O_3 wire. Both STEM images have been acquired at the regions marked with a white square in (b). Insets display atom resolution ADF images overlapped with ball model crystal structures in both cases. Oxygen atoms are hidden in the balls model. (c) Atomically resolved ADF image of the heterojunction projected onto the (001) and (10−1) planes of Ga_2O_3 and SnO_2, respectively, in the crossing wires structures. The projection of the Ga_2O_3 unit cell is drawn. The (400) planes in Ga_2O_3 and (101) planes in SnO_2 are also marked. (d) FFT of (c) that reveals lattice coincidence between {310} planes in Ga_2O_3 and {020} in SnO_2.

an epitaxial growth of SnO_2 nanoparticles along the NW with crystalline orientation matching with the Ga_2O_3 axis. The nucleation of these particles could be the out-diffusion of Sn impurities in the Ga_2O_3 NWs. As TEM results show, the surface facets of SnO_2 crystallites are {101} and {200} planes, which is in agreement with a minimization of surface energy in SnO_2.[34] On the other hand, Sn impurities could be eventually incorporated as well as dopant elements into the Ga_2O_3 NWs, as discussed below. These SK heterostructures remind the Ge nanoparticles on Si nanowire heterostructures, reported in refs 10 and 11, where the proposed driven mechanism was a Plateau−Rayleigh (P-R) instability of the Ge shell around the Si nanowires, to reduce the overall surface energy.[10,11] In addition, the strain due to the Si/Ge lattice mismatch was also suggested as an additional factor to modulate the final morphology of the heterostructures.[11] A strain-mediated growth has also been proposed in the long-range ordering of SiGe quantum dots on Si membranes.[35] In all those cases, the lattice mismatch was significant. We have shown that the [110] oriented Ga_2O_3 nanowires act as a lattice-matching "substrate" for the SnO_2 particles. On the other hand, a clear periodicity of SnO_2 particles around the NWs is not observed in our SKs, but the thickness of these particles seems to be homogeneous along the NW. This is in agreement with the P-R model where the diameter of the shell is determined by the time duration of the thermal treatment.[10]

The addition of chromium impurities in the precursors resulted into Ga_2O_3/SnO_2 CW growth. We have recently

DOI: 10.1021/acs.nanolett.6b04189
Nano Lett. XXXX, XXX, XXX−XXX

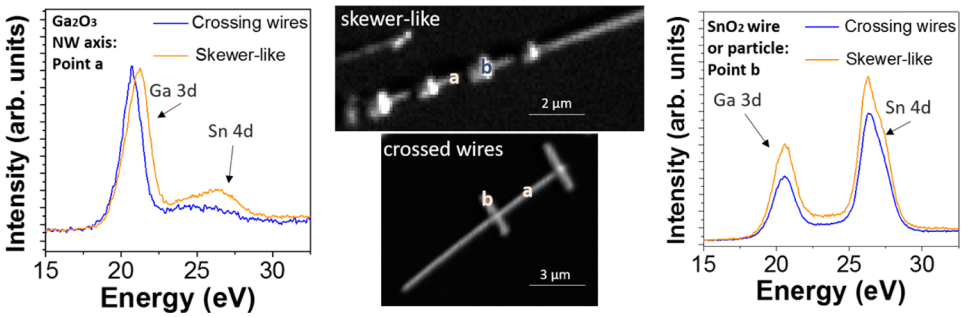

Figure 4. Left: XPS spectra obtained from the main Ga_2O_3 nanowire axis in crossing wires (blue line) and skewer-like structures (red line). Center: XPS Ga 3d map of both structures. Right: XPS spectra recorded at SnO_2 crossing wires (blue line) and at SnO_2 particles (red line).

reported this architecture[26] and made a characterization just at the junction point by means of X-ray absorption near edge structure (XANES) and extended X-ray absorption fine structure (EXAFS) analysis. The Cr concentration was found to be 0.014 ± 0.004 atom % Cr in Ga_2O_3, trunk, and below the detection limit in SnO_2 wires.[26] Here, we present the structural characterization performed by HRTEM. From side-view SEM images and EDX compositional analysis of these crossing NWs (Figure 1b,c, respectively), straight Ga_2O_3 NW and SnO_2 branches cutting across are easily revealed. The thickness of the Ga_2O_3 NW is of about 250 nm and its length is of several microns.

A focused ion beam (FIB) section, perpendicular to the Ga_2O_3 NW growth direction and containing a SnO_2 branch, was fabricated to elucidate the microstructure of the Ga_2O_3/SnO_2 heterojunction (see Figure 3a). Figure 3b (middle) corresponds to the annular dark-field (ADF) image with EDX elemental map superimposed (Ga in red and Sn in green) revealing the Ga_2O_3 NW and the SnO_2 branch in the FIB specimen. High-magnification ADF imaging taken in both SnO_2 and Ga_2O_3 (left and right panels, respectively) corresponds to the atomic structure along the [10−1] and [001], respectively. Therefore, the growth direction of the Ga_2O_3 wire has been identified as the [001] direction (along the electron beam) while the crossing SnO_2 wire grows perpendicularly to the Ga_2O_3 wire following the [−101] direction. This result reveals the different Ga_2O_3 growth direction in the SK with respect to the CW structures. The Ga_2O_3 growth direction is [110] in the former and [001] in the latter. Figure 3c shows an atomically resolved ADF image of the heterojunction projected onto the (001) and (10−1) planes of Ga_2O_3 and SnO_2 respectively in the CW structures. Figure 3d shows the Fourier transform of Figure 3c. Because there are two ordered lattices in the STEM image, there are two set of diffraction spots coming from both lattices. Diffraction spots associated with SnO_2 have been indexed in green and those corresponding to Ga_2O_3 are indexed in red. As it can be seen in the figure, some of these spots overlap. This overlapping reflects lattice coincidence between {310} planes in Ga_2O_3 and {020} planes in SnO_2.The image shows that both nanowires are joined by an interface boundary, which is not edge-on under these TEM conditions.

The structural analysis of the Ga_2O_3/SnO_2 CWs would help to get some insight into their formation. If we assume that the first step is the growth of the Ga_2O_3 NWs, we have to elucidate the reason for the growth of either SnO_2 nanowires across them or SnO_2 nanoparticles attached to them (shown above). The mechanism seems to be related to the particular growth direction of the Ga_2O_3 axis with the implications of this fact on the surface energy of the NWs facets. The obtained growth direction is [110] for NWs in SK nanostructures and [001] for NWs in the crossing Ga_2O_3/SnO_2 structures. The thermal treatments and source materials in both treatments were similar, except for the presence of chromium oxide in case of crossing structures. In the study by Chun et al. of Ga_2O_3 NW growth, it was found that the structure of the NW could be controlled with the use or not of the metal catalyst and that the nanowires grown with nickel as catalyst have random growth direction.[32] Here, the addition of a small amount of chromium into the source materials could have influenced the mobility and diffusion of the adsorbed species in the Ga_2O_3 primary NWs leading to [001] NWs instead of [110] ones when only gallium and tin were present. Moreover, a specific growth direction involves specific lateral surface planes of the NW, which implies that surface energy engineering could be used to control the final morphology of the nanostructures. It should be taken into account that we use a VS mechanism with no external catalyst. Crossing InSb nanowires have been obtained by a vapor−liquid−solid (VLS) method, which used gold as the catalyst, in a four-step process.[36] An example of combined nucleation and surface energy engineering to get tuned structures has been recently published in III−V nanowires,[12] where the provoked effect was the kinks formation in the GaAs NWs by modifying growth conditions. In this work, SnO_2 nanostructures are able to grow during the same thermal process. We have observed that the primary Ga_2O_3 wire orientation could serve as an engineering tool to get different architectures: (i) the growth of SnO_2 particles decorating the main thin Ga_2O_3 axis, leading to the skewers; or (ii) the growth of SnO_2 cross wires across the Ga_2O_3 wires.

In order to assess local optical and chemical properties of these complex morphologies, spatially resolved XPS and CL measurements have been carried out. CL in the SEM enables to probe electronic levels across the whole nanostructure (penetration depth of electron beam in the SEM is slightly lower than 1 μm for V_{acc} = 15 kV) while XPS measurements provides information about the electronic states and chemical bonding at the surface level.

XPS analysis with high spatial resolution has been performed at the ESCA microscopy line at Elettra synchrotron in Trieste. The operation conditions at this beamline balance quite well the trade-off between spatial and energy resolution. XPS spectra were performed with 648 eV photon energy. This means that kinetic energy of electrons is around 100−600 eV. Therefore, the mean free path (probe depth for XPS signal) is ∼10 Å. Hence, surface effects strongly influence the information on electronic properties. High-resolution XPS spectra were recorded to get the energy profiles of Ga 3d, Sn 4d, Sn 3d,

DOI: 10.1021/acs.nanolett.6b04189
Nano Lett. XXXX, XXX, XXX−XXX

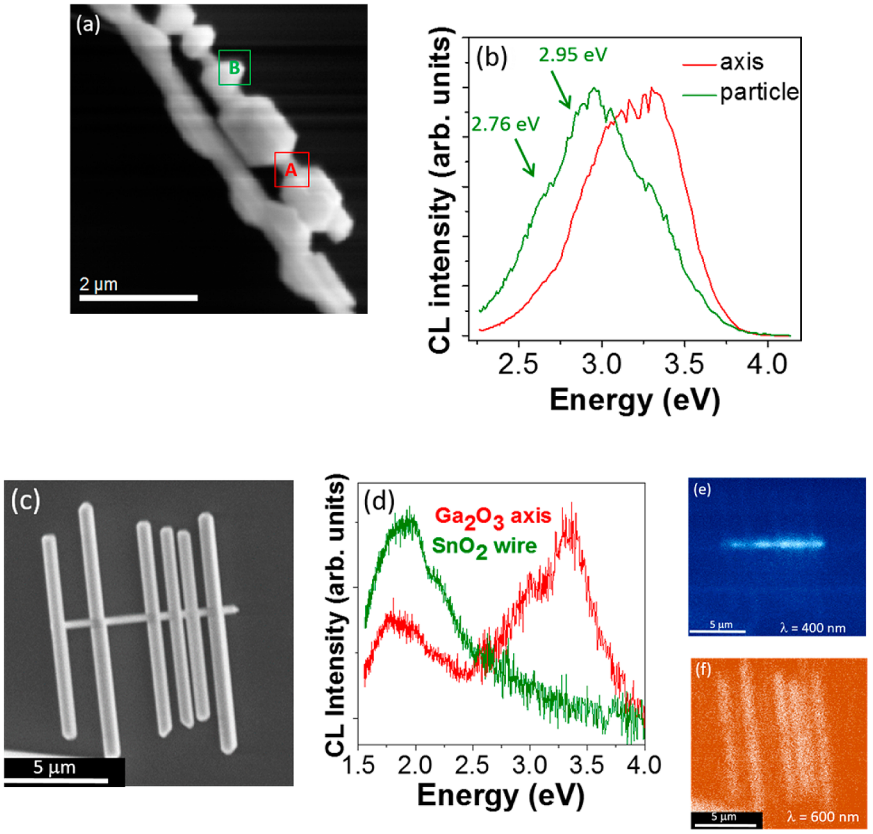

Figure 5. (a) Secondary electron image of SK structures. (b) CL spectra recorded at the points labeled as A and B corresponding to the Ga_2O_3 nanowire axis and the SnO_2 particle, respectively. (c) Secondary electron image of a CW structure. (d) CL spectra from Ga_2O_3 axis and one of the SnO_2 branches. (e) Monochromatic CL image at λ = 400 nm, and (f) monochromatic CL image at λ = 600 nm of the CW structure shown in (c).

and O 1s core levels, which gives information about the chemical bonding. Energy axis in high-resolution spectra was calibrated by fixing the C 1s binding energy (BE) at 248.8 eV.[37] Figure 4 summarizes the XPS results from the SK and CW architectures. Figure 4 (center) shows XPS maps representing the intensity of the Ga 3d line of both structures. High-resolution spectra from the central Ga_2O_3 axis in skewer-like structures and in cross wires are shown in Figure 4 (left: points marked as "a" in the XPS images). The binding energies for Ga 3d and Sn 4d core levels are 20.5 and 26.0 eV, respectively. We have selected this window energy because we can simultaneously obtain information about both elements in the same experiment. The results show the main Ga 3d peak in the axis of both nanostructures but in the SK structures a non-negligible peak is observed at 26 eV that corresponds to the Sn 4d binding energy level. The Ga 3d binding energy of 20.5 eV corresponds to the Ga^{3+} in the Ga—O bonding in undoped material.[38] A slight shift toward higher energies is observed in the XPS spectrum of point "a" in the skewer axis (Figure 4 (left)). This would be consistent with the presence of Sn in the skewer axis as dopant but not in the axis of CWs. Alternatively, spectra from the SnO_2 particles and SnO_2 cross wires have also been obtained from XPS maps (points marked as "b") and displayed at the right in Figure 4 (right). The dominant peak corresponds to the Sn 4d line, but it is worth noticing that the Ga 3d line is rather important in both SnO_2 particles and nanowires. This result shows that both nanowires and nanoparticles are Ga doped, at least at the surface level. XPS spectra of the Sn $3d_{5/2}$ and O 1s lines have also been recorded (Figure S4 in the Supporting Information). The XPS analysis has also revealed a small peak at 487 eV (Sn $3d_{5/2}$ level) in the Ga_2O_3 axis of the SKs and changes in the line profile of the O 1s levels. Hence, these XPS results suggest that the Ga_2O_3 nanowire axis in the SKs are slightly Sn doped while the axis in CWs seem to be undoped.

Finally, we have investigated the luminescence of both kinds of nanostructures, SK and CW, by means of CL. The high spatial resolution of the CL technique enables one to get local CL spectra at different points in the structures. Because the quantum efficiency of both Ga_2O_3 and SnO_2 is rather high, all the CL measurements have been carried out at room temperature. Even though semiconductor oxides exhibit a wide bandgap, visible luminescence occurs quite often due to the presence of oxygen vacancies that give rise to luminescence centers. In many cases, the oxygen vacancies may form complex defects with other point defects or impurities, which makes the visible luminescence bands rather broad.

Figure 5a shows the secondary electron image of a SK structure where "A" label stands for axis and "B" label for particles. Figure 5b shows the spectra acquired at the Ga_2O_3 axis and at the tip of one of the SnO_2 particles attached to the main NW in the SK structures. The CL emission from Ga_2O_3 corresponds to the ultraviolet (UV) band composed of two components (3.3 and 3.0 eV) related to bound excitons and donor−acceptor pair with (DAP) transitions.[39] Both donor and acceptor centers involve native point defects with the oxygen vacancy V_O generally accepted to act as the donor center, while $V_{Ga}-V_O$ complexes are considered to be acceptors.[40] This emission is characteristic of undoped Ga_2O_3. CL spectra of pellets of Ga_2O_3 and SnO_2 oxides, which have been used as

DOI: 10.1021/acs.nanolett.6b04189
Nano Lett. XXXX, XXX, XXX−XXX

reference samples, with their usual native-defects related UV and visible bands, respectively, are displayed in the Figure S5 (Supporting Information). It can be seen that the CL spectrum from the axis wire (spectrum A) is quite similar to that shown in Figure S5. On the other hand, known luminescence bands in SnO_2 are the orange (OR) band at 1.95 eV (635 nm), related to oxygen vacancies, and a green−blue (GB) band, which is strongly dependent on surface states.[41] Several GB bands at 2.25 and 2.58 eV (550 and 480 nm) have been reported in SnO_2 microcrystals with relative intensities dependent on surface facets and thermal treatments.[42] In our case, the CL emission of the SnO_2 particles exhibits the GB band and blue emission composed of several bands (2.76 and 2.95 eV), which is unusual. No significant orange emission is found in the SnO_2 particles. Similar blue-UV emission has been reported in SnO_2 nanoparticles and attributed to quantum confinement effects,[43] which can be ruled out here because the SnO_2 particles in the skewer structures are around 800−900 nm. However, the particles display well-defined facets that may have characteristic surface states.[41] This could explain the observed blue-UV emission and the quenching of the orange band.

A CL analysis of the crossed Ga_2O_3−SnO_2 wires is summarized in Figure 5c−f. Figure 5c shows the secondary electron image of a CW assembly. CL emission from Ga_2O_3 axis shows the characteristic UV band but also a non-negligible broad band in the orange region (Figure 5d). On the other hand, the orange band (1.95 eV) dominates the CL spectrum from the SnO_2 wires. As it has been mentioned, this OR band is commonly attributed to oxygen vacancies in SnO_2 bulk material.[44] Therefore, the CL emission from the SnO_2 wires crossing the Ga_2O_3 axis is dominated by native defects instead of surface states, which is in contrast to the emission of SnO_2 particles in the skewer-like structures, where the main CL bands are those of the blue-UV region. These results agree with the above-described structural and surface analysis. Monochromatic CL images of the characteristic emission bands of both Ga_2O_3 axis and SnO_2 wires are displayed in Figure 5e,f. The main ultraviolet emission comes from the central trunk, while crossing wires are emitting orange light. In addition, the orange light that arises in the main Ga_2O_3 axis could come from waveguiding luminescence of the SnO_2 cross wires. The luminescence results demonstrate a dependence on the shape of the luminescence properties in the case of SnO_2. Therefore, shape engineering could be a useful approach to capitalize the plenty of possibilities of semiconductor oxides assemblies.

In summary, the Ga_2O_3−SnO_2 material system has been revealed as a platform to study orientation-dependent architectures and properties. A thermal evaporation method at high temperature, close to the melting points of both oxides, allows the formation of either SK structures or CW. The root of these architectures is a primary Ga_2O_3 nanowire with a preferred growth direction. In the SK structures, Sn out-diffusion in the [110] Ga_2O_3 NWs may nucleate the formation of SnO_2 particles further developed with a nice lattice matching between the surface axis and the particles. The observed facets in the SnO_2 particles are compatible with minimum surface energy considerations. On the other hand, the addition of a small amount of chromium oxide in the source materials leads to the formation of crossed Ga_2O_3−SnO_2 wires. In this case, the growth direction of the Ga_2O_3 nanowires is the [001], probably induced by the presence of chromium. In this scenario, Sn impurities in the main Ga_2O_3 axis seem to act as nucleation sites for SnO_2 wires at some points of the main axis in a secondary growth self-catalyzed scheme. The Ga_2O_3/SnO_2 junction in CW structures examined by HRTEM has been revealed as a grain boundary and it seems that the lattice matching condition is not required for the formation of the CW structures. XPS results demonstrate the presence of a small amount of Sn in the main Ga_2O_3 axis of skewer structures, not observed in the Ga_2O_3 axis of the crossing wires. On the other hand, CL emission of SnO_2 has been shown to be affected by its shape and dimensions of the structures. Both assemblies show luminescence at room temperature. While CL of SnO_2 wires in the cross structures is dominated by the orange band, the CL emission of SnO_2 particles is dominated by blue emission that probably originated by the exposure of specific surface facets with characteristic surface states.

■ ASSOCIATED CONTENT

Supporting Information

The Supporting Information is available free of charge on the ACS Publications website at DOI: 10.1021/acs.nanolett.6b04189.

Additional figures (PDF)

In situ video growth of Ga_2O_3/SnO_2 nanostructures (AVI)

■ AUTHOR INFORMATION

Corresponding Authors

*E-mail: a.m.sanchez@warwick.ac.uk.

*E-mail: bianchi@ucm.es.

ORCID

Bianchi Méndez: 0000-0002-6289-7437

Author Contributions

The manuscript was written through contributions of all authors. All authors have given approval to the final version of the manuscript.

Notes

The authors declare no competing financial interest.

■ ACKNOWLEDGMENTS

This work has been supported MINECO (projects CSD 2009-00013, MAT 2012-31959, MAT 2015-65274-R-FEDER). We thank Richard Beanland for his advice at Warwick University. We also thank Luca Gregoratti for his assistance at ESCA microscopy beamline at Elettra Sincrotrone. Bianchi Méndez acknowledges the mobility Grant supported by MEC (PRX14/00134) for sabbatical leave at Warwick University.

■ REFERENCES

(1) Li, C.; Yu, Y.; Chi, M.; Cao, L. *Nano Lett.* **2013**, *13*, 948−953.

(2) Borgström, M. T.; Zwiller, V.; Müller, E.; Imamoglu, A. *Nano Lett.* **2005**, *5*, 1439−1443.

(3) Liu, Q.; Lu, H.; Shi, Z.; Wu, F.; Guo, J.; Deng, K.; Li, L. *ACS Appl. Mater. Interfaces* **2014**, *6*, 17200−17207.

(4) Lu, J. G.; Chang, P.; Fan, Z. *Mater. Sci. Eng., R* **2006**, *52*, 49−91.

(5) Wang, Z. L. *Adv. Mater.* **2003**, *15*, 432−436.

(6) Huang, M. H.; Mao, S.; Feick, H.; Yan, H.; Wu, Y.; Kind, H.; Weber, E.; Russo, R.; Yang, P. *Science* **2001**, *292*, 1897−1899.

(7) Lieber, C. M.; Wang, Z. L. *MRS Bull.* **2007**, *32*, 99−108.

(8) Sirbuly, D. J.; Tao, A.; Law, M.; Fan, R.; Yang, P. *Adv. Mater.* **2007**, *19*, 61−66.

(9) Varley, J. B.; Janotti, A.; Franchini, C.; Van de Walle, C. G. *Phys. Rev. B: Condens. Matter Mater. Phys.* **2012**, *85*, 081109.

DOI: 10.1021/acs.nanolett.6b04189
Nano Lett. XXXX, XXX, XXX−XXX

(10) Day, R. W.; Mankin, M. N.; Gao, R.; No, Y.-S.; Kim, S.-K.; Bell, D. C.; Park, H.-G.; Lieber, C. M. *Nat. Nanotechnol.* **2015**, *10*, 345−352.
(11) Day, R. W.; Mankin, M. N.; Lieber, C. M. *Nano Lett.* **2016**, *16*, 2830−2836.
(12) Yuan, X.; Caroff, P.; Wong-Leung, J.; Fu, L.; Tan, H. H.; Jagadish, C. *Adv. Mater.* **2015**, *27*, 6096−6103.
(13) Lv, C.; Peng, Z.; Zhao, Y.; Huang, Z.; Zhang, C. J. *J. Mater. Chem. A* **2016**, *4*, 1454−1460.
(14) Hou, J.; Qu, Y.; Krsmanovic, D.; Ducati, C.; Eder, D.; Kumar, R. V. *J. Mater. Chem.* **2010**, *20*, 2418−2423.
(15) Cheng, J. J.; Nicaise, S. M.; Berggren, K. K.; Gradecak, S. *Nano Lett.* **2016**, *16*, 753−759.
(16) Hidalgo, P.; Méndez, B.; Piqueras, J. *Nanotechnology* **2005**, *16*, 2521−2524.
(17) Díaz-Guerra, C.; Piqueras, J. *Cryst. Growth Des.* **2008**, *8*, 1031−1034.
(18) Alemán, B.; Fernández, P.; Piqueras, J. *Appl. Phys. Lett.* **2009**, *95*, 013111.
(19) Maestre, D.; Häussler, D.; Cremades, A.; Jäger, W.; Piqueras, J. *J. Phys. Chem. C* **2011**, *115*, 18083.
(20) Jin, S.; Wang, X.; Wang, X.; Ju, M.; Shen, S.; Liang, W.; Zhao, Y.; Feng, Z.; Playford, Y. L.; Walton, R. I.; Li, C. *J. Phys. Chem. C* **2015**, *119*, 18221−18228.
(21) López, I.; Castaldini, A.; Cavallini, A.; Nogales, E.; Méndez, B.; Piqueras, J. *J. Phys. D: Appl. Phys.* **2014**, *47*, 415101.
(22) Martinez, C. J.; Hockey, B.; Montgomery, C. B.; Semancik, S. *Langmuir* **2005**, *21*, 7937−7944.
(23) Abd-Ellah, M.; Bazargan, S.; Thomas, J. P.; Rahman, M. A.; Srivastava, S.; Wang, X.; Heining, N. F.; Leung, K. T. *Adv. Electron. Mater.* **2015**, *1*, 1500032.
(24) Mazeina, L.; Picard, Y. N.; Maximenko, S. I.; Perkins, F. K.; Glaser, E. R.; Twigg, M. E.; Freitas, J. A.; Prokes, S. *Cryst. Growth Des.* **2009**, *9*, 4471−4479.
(25) Hsu, C. L.; Lu, Y. C. *Nanoscale* **2012**, *4*, 5710.
(26) Martínez-Criado, G.; Segura-Ruiz, J.; Chu, M. H.; Tucoulou, R.; López, I.; Nogales, E.; Mendez, B.; Piqueras, J. *Nano Lett.* **2014**, *14*, 5479−5487.
(27) Hidalgo, P.; Méndez, B.; Piqueras, J. *Nanotechnology* **2008**, *19*, 455705.
(28) Cebriano, T.; Ortega, Y.; Hidalgo, P.; Maestre, D.; Méndez, B.; Piqueras, J. *Nanotechnology* **2014**, *25*, 235701.
(29) López, I.; Nogales, E.; Méndez, B.; Piqueras, J.; Peche, A.; Ramirez-Castellanos, J.; González-Calbet, J. *J. Phys. Chem. C* **2013**, *117*, 3036−3045.
(30) Lu, J. G.; Chang, P.; Fan, Z. *Mater. Sci. Eng., R* **2006**, *52*, 49−91.
(31) Ueda, N.; Hosono, H.; Waseda, R.; Kawazoe, H. *Appl. Phys. Lett.* **1997**, *71*, 933.
(32) Chun, H. J.; Choi, Y. S.; Bae, S. Y.; Seo, H. W.; Hong, S. J.; Park, J.; Yang, H. *J. Phys. Chem. B* **2003**, *107*, 9042−9046.
(33) Hosein, I. D.; Hegde, M.; Jones, P. D.; Chirmanov, V.; Radovanovic, P. V. *J. Cryst. Growth* **2014**, *396*, 24−32.
(34) Batzill, M.; Diebold, U. *Prog. Surf. Sci.* **2005**, *79*, 47−154.
(35) Ritz, C. S.; Kim-Lee, H.-J.; Detert, D. M.; Kelly, M. M.; Flack, F.; Savage, D. E.; Cai, Z.; Evans, P. G.; Turner, K. T.; Lagally, M. G. *New J. Phys.* **2010**, *12*, 103011.
(36) Plissard, S. R.; van Weperen, I.; Car, D.; Verheijen, M. A.; Immink, G. W. G.; Kammhuber, J.; Cornelissen, L. J.; Szombati, D. B.; Geresdi, A.; Frolov, S. M.; Kouwenhoven, L. P.; Bakkers, E. P. A. M. *Nat. Nanotechnol.* **2013**, *8*, 859−864.
(37) Miller, D. J.; Biesinger, M. C.; McIntyre, N. S. *Surf. Interface Anal.* **2002**, *33*, 299.
(38) López, I.; Utrilla, A.; Nogales, E.; Méndez, B.; Piqueras, J.; Peche, A.; Ramirez-Castellanos, J.; González-Calbet, J. *J. Phys. Chem. C* **2012**, *116*, 3935.
(39) Binet, L.; Gourier, D. *J. Phys. Chem. Solids* **1998**, *59*, 1241−1249.
(40) Shimamura, K.; Víllora, E. G.; Ujiie, T.; Aoki, K. *Appl. Phys. Lett.* **2008**, *92*, 201914.
(41) Yuan, X. L.; Lazzarini, L.; Salviati, G.; Zha, M.; Sekiguchi, T. *Mater. Sci. Semicond. Process.* **2006**, *9*, 331−336.
(42) Maestre, D.; Cremades, A.; Piqueras, J. *J. Appl. Phys.* **2005**, *97*, 044316.
(43) Das, S.; Kar, S.; Chaudhuri, S. *J. Appl. Phys.* **2006**, *99*, 114303.
(44) Maestre, D.; Cremades, A.; Piqueras, J. *J. Appl. Phys.* **2004**, *95*, 3027.

DOI: 10.1021/acs.nanolett.6b04189
Nano Lett. XXXX, XXX, XXX−XXX